JOURNAL OF AGRICULTURAL AND FOOD CHEMISTRY

Agricultural and Environmental Chemistry

Fabrication of Furan-Functionalized Quinazoline Hybrids: Their Antibacterial Evaluation, Quantitative Proteomics, and Induced Phytopathogen Morphological Variation Studies

Qing-Su Long, Li-Wei Liu, Yong-Liang Zhao, Peiyi Wang, Biao Chen, Zhong Li, and Song Yang

J. Agric. Food Chem., **Just Accepted Manuscript** • DOI: 10.1021/acs.jafc.9b03419 • Publication Date (Web): 18 Sep 2019

is published by the American Chemical Society. 1155 Sixteenth Street N.W., Washington, DC 20036

Fabrication of Furan-Functionalized Quinazoline Hybrids: Their Antibacterial Evaluation, Quantitative Proteomics, and Induced Phytopathogen Morphological Variation Studies

Qing-Su Long [a], Li-Wei Liu [a], Yong-Liang Zhao [a], Pei-Yi Wang* [a], Biao Chen [a], Zhong Li [b], Song Yang* [a,b]

[a] State Key Laboratory Breeding Base of Green Pesticide and Agricultural Bioengineering, Key Laboratory of Green Pesticide and Agricultural Bioengineering, Ministry of Education, Center for R&D of Fine Chemicals of Guizhou University, Guiyang, 550025, China.

[b] College of Pharmacy, East China University of Science & Technology, Shanghai, China 200237.

* Corresponding author.

E-mail: jhzx.msm@gmail.com (S. Yang), pywang888@126.com (P.-Y. Wang)

Abstract

The limited number of agrochemicals targeting plant bacterial diseases has driven us to develop highly efficient, low-cost, and versatile antibacterial alternatives. Herein, a novel type of simple furan-functionalized quinazolin-4-amines was systematically fabricated and screened for their antibacterial activity. Bioassay results revealed that compounds **C_1** and **E_4** could substantially block the growth of two frequently-mentioned pathogens *Xanthomonas oryzae* pv. *oryzae* and *X. axonopodis* pv. *citri in vitro*, displaying appreciable EC_{50} values of 7.13 and 10.3 mg/L, respectively. This effect was prominently improved by comparing those of mainly used agrochemicals. *In vivo* experiment against bacterial blight further illustrated their viable applications as antimicrobial ingredients. Quantitative proteomics demonstrated that **C_1** possessed a remarkable ability to manipulate the upregulation and downregulation of expressed proteins, which probably involved D-glucose and biotin metabolic pathways. This finding was substantially verified by parallel reaction monitoring analysis. Scanning electron microscopy images and fluorescence spectra also indicated that the designed compounds had versatile capacities for destroying the integrity of bacteria. Given these remarkable characteristics, furan-functionalized quinazoline hybrids can serve as a viable platform for developing innovative antibiotic alternatives against bacterial infections.

Keywords

quinazolin-4-amines, furan group, antibacterial, quantitative proteomics

1. Introduction

Plant pathogenic bacteria have received global attention and are extensively studied for their substantial threats toward agricultural production.[1-4] They can attack and infect a variety of important crops, which results in serious diseases, including rice bacterial blight,[5,6] various cankers,[7,8] cabbage soft rot,[9] and tobacco bacterial wilt.[10] These diseases directly lead to huge losses in agricultural economy each year and have become some of the most rapidly emerging challenges and urgent issues that must be addressed.[11,12] Currently, chemical therapy utilizing antibiotic drugs serves as one of the most efficient and cost-effective strategies and has made great contributions in preventing and controlling bacterial diseases.[13,14] However, there is a limited number of agrochemicals targeting plant bacterial diseases, including zhongshengmycin, bismerthiazol (**BT**, is now being reevaluated), thiodiazole copper (**TC**), Zn thiazole, and kocide.[4,6,15] Moreover, the emergence of drug-resistant pathogenic bacterial strains has resulted in significant difficulties in agriculture because some pathogens can undergo elusive and expeditious variation against extrinsically enforced attacks originating from various factors such as climate change, bacterial transformations, usual treatment methods, and long-term application of commercial bactericides.[16,17] Such resistant strains are capable of making quick and adequate responses against common commercial agents after forming defense mechanisms, which further aggravates the difficulty for managing this situation and increases health risks.[18] Thus, novel and highly efficient antibiotic surrogates that can attack pathogens through unique modes of action or disable bacterial resistance to

treatment must be discovered and developed.

The search for a simple structural architecture with highly efficient bioactivity and short synthesis will be prioritized for the future development of commercial pesticides in agriculture.[19] At present, the agriculture industry has put forward the following requirements for developing modern agrochemicals: good biocompatibility and degradability, eco-friendly, target selectivity, and insignificant cytotoxicity.[20] Considering above factors, the selection of molecular skeleton for exploring highly efficient antibiotic surrogates has received considerable attentions. Quinazoline skeleton, which belongs to the *N*-containing heterocyclic building block, has drawn considerable attention in the synthesis and bioactivity research.[21] Its derivatives displays wide spectrum of pharmaceutical activities, including anticancer, antimicrobial, anti-inflammatory, anti-adenovirus, anti-oxidative, and other activities.[22-30] Because the quinazoline fragment owns a vital status in predicting the biological behaviors of a title molecule, considerable investigations have been performed on this flexible motif, which have led to an array of quinazoline-tailored compounds with practical and substantial applications in many fields (Figure 1a). For instance, gefitinib,[31] erlotinib,[32] canertinib,[33] and lapatinib ditosylate[34] with quinazoline patterns have already been introduced into the market for the treatment of human cancers. Fluquinconazole has been successfully developed as a powerful systemic fungicide against plant fungal diseases caused by pathogenic Basidiomycetes, Hymenomycetes, and Ascomycetes.[35] Further antifungal mechanism studies elucidated that fluquinconazole serves as a sterol demethylation inhibitor that

destroys and prevents the biosynthesis of ergosterol, which is an important component of bacterial cell membrane. Fenazaquin was the first discovered pesticide with good acaricidal activity against *Eutetranychus*, *Panonychus*, *Tetranychus cinnabarinus*, and *Brevipalpus phoenicis* and was subsequently exploited as an acaricide by Dow-Elanco.[36] Pyrifluquinazon is an insecticide for whitefly, aphids, and scale insects from vegetables, fruits, and tea leaves.[37] Besides these commercialized pesticides, abundant promising compounds based on quinazoline skeletons were reported and bioassayed with augmented biological silhouettes, especially in the antibacterial field. For example, Manetsch et al. have synthesized and evaluated the antimicrobial activity of diverse N^2,N^4-disubstituted quinazoline-2,4-diamines and found that these designed compounds have good antibiotic ability against multidrug resistant *Staphylococcus aureus*.[38] Gottasová et al. reported 2,6-disubstituted 4-aniloquinazolines with excellent antibacterial activity against *Bacillus subtilis* and *S. aureus* with the lowest EC_{50} values of 0.7 and 0.8 μg/mL, respectively.[39] Chandrika et al. have constructed and biologically tested a type of 2,4,6-trisubstituted quinazolines, providing permissible antibiotic functions toward different kinds of Gram-positive and Gram-negative bacterial strains.[40] Inspired by the abovementioned studies, rational modification based on the quinazoline skeleton should promote the discovery of bioactive substrates with excellent performance owing to the versatile functions of this valuable moiety.

Additionally, the bioactive substructure furan scaffold has multi-functional pharmacological features in its integrated molecular architectures and has been

104 extensively explored and identified with various applications (Figure 1a).[41,42]
105 Commercial agents such as furalaxyl, fenfuram, furcarbanil, methfuroxam, and
106 cyclafuramid have been exploited as effective fungicides in agriculture to manage a
107 range of plant fungal diseases.[43,44] Furamizole is being developed as an antibiotic
108 agent in late stage clinical trials.[45] In addition, resmethrin and proparthrin, which are
109 widely used as insecticidal agents that contain typical furan moieties, are potent
110 against housefly, mosquito larvae, and cockroach.[46] Meanwhile, flurtamone, one of
111 the classical furan derivatives, has been used as a herbicide for inhibiting carotenoid
112 synthesis.[47] Given that the furan building block plays a significant role in drug-design
113 programs, continuous efforts and studies have been dedicated to the design of
114 furan-tailored molecules, which provide a new avenue for addressing plant bacterial
115 diseases.

116 Considering the limitations of existing bactericides with single mode of action,
117 the emergence of drug-resistant plant pathogenic bacteria, the difficulty of producing
118 drugs, the cost of manufacturing in agriculture, and the aforementioned valuable
119 building blocks of quinazoline and furan fragments, a type of simple molecular
120 structure with versatile quinazoline and furan patterns was fabricated through facile
121 bridging linkers in this study (Figure 1b). These designed compounds could be
122 integrated and endowed with the properties of quinazoline and furan, including
123 antibacterial capacity and specific ability to attack pathogens through different modes
124 of action. Thus far, studies that detect the antibiotic capability of furan-tailored
125 quinazolin-4-amines toward plant pathogens are lacking. In the present study, two

invasive and widespread phytopathogenic bacterial strains including *Xanthomonas oryzae* pv. *oryzae* (*Xoo*) and *X. axonopodis* pv. *citri* (*Xac*), which can cause bacterial blight and citrus bacterial canker, respectively, were tested *in vitro*. Subsequently, *in vivo* testing was carried out to further identify the prospective application for developing the furan-tailored quinazolin-4-amines as agricultural agents. Subsequently, label-free proteomic analysis was exploited to monitor the upregulation and downregulation of expressed proteins induced by hyperactive compounds.[48-50] SEM frames would be provided to investigate the topological variations of pathogens after incubation with obtained molecules.[51]

2. Materials and methods

2.1 Instruments and Chemicals

NMR data were recorded by AVANCE III HD 400 and JEOL-ECX-500 devices. TMS is the internal standard, DMSO-d_6 or $CDCl_3$ is solvent. Chemical shifts and coupling constants (*J*) were expressed in parts per million (ppm) and Hz, respectively. HRMS spectra was determined by a Thermo Scientific Q Exactive in CH_3OH. The instrument Nova Nano SEM 450 was employed to monitor the changes of bacterial morphology.

2.2 *In vitro* antimicrobial assay

In vitro inhibitory effects against *Xoo* and *Xac* of title compounds were carried out by exploiting the turbidimeter test.[51] In this experiment, **BT**, **TC**, and DMSO were used as the positive and blank controls, respectively. NB medium (pH 7.0–7.2) was prepared by mixing 10.0 g glucose, 1.0 g yeast powders, 5.0 g peptone and 3.0 g beef

148 extracts in 1.0 L deionized water. Briefly, pathogen *Xoo* (or *Xac*) was cultivated in
149 NB medium until reaching to the logarithmic phase. Then 40 μL bacteria were added
150 into the testing tube containing various dosages of title molecules in 5 mL NB
151 medium. The concentrations of 100 and 50 μg/mL were chosen for primarily
152 bioassays. While the drug concentrations, for example, 50, 25, 12.5, 6.25, 3.125
153 μg/mL (were gradually reduced two-folds), were used for EC_{50} calculation. All the
154 samples were put in the shaker and cultivated for 24-48 hours at the prescriptive
155 conditions (temp. 28±1 °C, 180 rpm) until the blank control reached to the
156 logarithmic phase. Then the turbidity of 200 μL pipetted bacterial sample was
157 monitored by a multiskan ascant at 595 nm. The final corrected OD_{595} data (T or C; T
158 is the sample containing drugs, C is the sample containing the equivalent DMSO
159 solvent) was obtained by subtracting the turbidity of the background of medium
160 without pathogens. The inhibitory value (*I*) was gained by following the formula: *I*
161 (%) = (C−T)/C × 100. And the related EC_{50} values were calculated by utilizing the
162 SPSS 17.0 software based on the inhibitory values at various drug dosages. Three
163 sample replications were used in this study.

164 **2.3 *In vivo* antibacterial assay**

165 Title molecules $\mathbf{B_2}$ and $\mathbf{C_1}$ were selected to examine the substantial effects against rice
166 bacterial blight.[6] Meanwhile, the mainly used bactericides **BT** (20% wet powder) and
167 **TC** (20% SC) were considered as positive controls. Rice variety 'Fengyouxiangzhan'
168 was planted for about 8 weeks to start testing their therapeutic and protective effects.
169 For the curative performance, an aseptic scissor dipped with *Xoo* cells was used to

infect rice leaves. One day later, **B_2** and **C_1** with a drug concentration of 200 μg/mL were evenly sprayed on leaves. Meanwhile, the drug-free solution was used for the negative group. All the treated plants were cultured in the constant temperature (28 °C) and humidity (90% RH) incubator for 14 days before testing the disease index. For the protective effects, the difference was that the drug solution with the same dosage was firstly sprayed before inoculation with *Xoo* cells. The related disease index could be obtained after 14 days. The corresponding control efficiencies (*I*) were provided according to the formula: $I = (C\text{-}T)/C \times 100\%$. C and T represent the disease index of negative and drug-treated controls, respectively.

2.4 Quantitative proteomics bioassay

Collection of *Xoo* cells

Compound **C_1** (EC_{50} = 7.13 μg/mL) towards pathogen *Xoo* was used for the label-free quantitative proteomics analysis. *Xoo* cells was cultured in obove-mentioned NB medium until the turbidity (OD_{595}) attained to 0.1. Then, **C_1** with a dosage of $5\times EC_{50}$ was added and incubated with *Xoo* for about 6 h under the same conditions unitil the turbidity (for the drug-free group) came up to 0.6-0.8. Finally, *Xoo* cells were gathered at 8000 rpm at 4 ^{o}C for standby.

LC-MS/MS Analysis

The extracted total proteins from *Xoo* cells were gradually digested by trypsin to provide the peptide sample, which then was dissolved by 0.1% HCOOH. The obtained solution was loaded into RP column with the length of 0.15 meter. The separation was carried out on the EASY-nLC 1000 UPLC with a fixed flow velocity

192 (0.4 μL/min). Subsequently, the peptide ingredients were analyzed by Q Exactive TM
193 apparatus with EV of 2.0 kV.

194 **Database Search**

195 Maxquant search engine (v.1.5.2.8) and tandem mass spectra were used to deal with
196 these obtained MS data. The special cleavage enzyme Trypsin/P could have two
197 missing cleavages. For the primary and main search, the mass tolerance for pioneer
198 ions were arranged as the corresponding 20.0 and 5.0 ppm. Meanwhile, the mass
199 limitoferror of fragment ions was installed as 2×10^{-2} Da. The special
200 carbamidomethyl and oxidation toward the corresponding cysteine and methionine
201 were appointed as fixed and mutable modifications, respectively. The FDR and
202 minimal score for peptides were installed as < 0.01 and > 40.0, respectively.

203 **Bioinformatics Methods**

204 Gene Ontology (GO) annotation proteome from UniProt-GOA database (www.
205 http://www.ebi.ac.uk/GOA/) was used to classify these obtained proteins. There were
206 3 categories in GO annotation, such as molecular function (MF), cellular compartment
207 (CC), and biological process (BP). The wolfpsort was utilized to forecast subcellular
208 localization. The enriched pathways were obtained and confirmed by KEGG database
209 (https://www.kegg.jp/kegg/kegg2.html). For protein-protein interactions, the whole
210 differentially expressed protein database accession or sequence were searched against
211 the STRING database version 10.5.

212 **2.5 SEM patterns of pathogens**

213 Pathogens *Xoo* (or *Xac*) were cultured in NB medium until the turbidity (OD_{595})

attained to 0.6. Then 1.5 mL bacteria solution was pipetted for centrifugation (7000 rpm, 5 min) to remove the NB medium. The obtained cells were washed by PBS buffer (pH 7.2) three times and re-dissolved with 1.50 mL PBS solution. Later, these cells were incubated with compounds **C_1** and **E_4** at the concentration of 50.0 μg/mL, 100.0 μg/mL, and the same amount of DMSO for 10 h at 28℃. After that, every specimen was centrifuged and washed with PBS solution 3 times. Next, these pathogens were immobilized by 2.5% glutaraldehyde solution for 8 hours at 4℃. The obtained cells were dehydrated with gradient ethanol solution and absolute tert-butanol, respectively. Finally, all the samples were freezing dried and coated with gold before imaging.

2.6 PI uptake assay

Briefly, 1.0 mL of bacteria *Xoo* (or *Xac*) cultured at the logarithmic phase were prepared and treated with **C_1** (or **E_4**) at various concentrations for 12 hours at 28℃, while the same amount of DMSO was used as the solvent control. Then 5 μL of 2 g/L propidium iodide (PI) was added to the solution and cultured for 15 min. After that, uptake of PI was measured using a Fluoromax-4cp Fluorescence Spectrophotometer.

3. Results and Discussion

To investigate the effect of fusion of quinazoline and furan fragments on bioactivity, we first designed and constructed a furan-tagged quinazolin-4-amine that was bridged with a methylene amino linker (Figure 2). In brief, 6-bromo-4-chloroquinazoline was treated with 1-(2-furyl)methylamine in isopropanol solution to provide the target compound **A_1** with the yield of 82.0%, which was subsequently characterized by

NMR and HRMS.[52] To obtain different types of molecules for bioactive comparison, the furan ring was replaced with a benzene ring, 4-fluorophenyl, and 3-pyridyl groups to provide the corresponding title compounds **A_2**, **A_3**, and **A_4** via the same synthetic protocol for **A_1**. Turbidimeter test was used to determine the antibacterial potency against *Xoo* and *Xac*, while the mainly applied agricultural antibiotic drugs **BT** and **TC** were analyzed as the comparison agents. Preliminary biological activity results (Table 1) suggested that **A_1** with furan moiety could selectively and completely suppress the growth of *Xoo* at 25 and 50 μg/mL. Thus, the combination of the two building blocks in a single molecular architecture could contribute to the discovery of bioactive substrates. Surprisingly, an opposite scene was discovered for the bioactivity of **A_2**, **A_3**, and **A_4** against *Xoo*, confirming the excellent property of the bioactive furan scaffold. To determine whether the introduction of a substituted group on the furan ring affected anti-*Xoo* activity, **A_5** with a methyl motif at the 5-position of furan ring was synthesized. The antibacterial potency was significantly decreased from the inhibition rate of 100% to 40.0% after the variation, suggesting that a sterically hindered methyl group could block additional interactions targeting bacterial receptors. According to the principle of equal arrangement of electrons, **A_6** with a thiofuran part was fabricated, and its bioactivity was evaluated. However, the antibacterial power was not attained, confirming the crucial role of furan moiety toward biological action. To clarify the potential function of amino group toward bioactivity, **A_7** was synthesized by replacing the NH with a sulfur atom. A similarly reduced antibiotic efficiency was obtained, revealing that the amino group may serve

as a hydrogen bond donor or basic group that promotes enhanced interactions with the bacterial receptors. For anti-*Xac* activity, all the compounds displayed weak inhibition effects at 100 μg/mL, although both *Xoo* and *Xac* are Gram-negative bacteria. **A_1** with the strongest antibacterial activity was considered as the secondary leading compound for further molecular structure optimization.

Given that **A_1** had excellent potential as antibacterial indicator, the bioactivity of the secondary amine substituents was investigated. **A_1** reacted with iodomethane, iodoethane, iodopropane, iodobutane, or 4-fluorobenzyl bromide under the strong NaH base in dry *N*,*N*-dimethylformamide solution to obtain the corresponding compounds **B_1–B_5** as confirmed by the results of NMR and HRMS (Figure 3). The bioassay result is shown in Table 2 and reveals that the substituents located at the *N*-position significantly influenced bioactivity. The EC_{50} values had the following trend: an initial increase after NH was changed (**A_1**, 9.77 μg/mL) to NCH_3 (**B_1**, 14.1 μg/mL), a decrease via the introduction of an ethyl group (**B_2**, 7.03 μg/mL), and an increase along with extending alkyl chain lengths (**B_3**, propyl, 21.7 μg/mL; **B_4**, n-butyl, 31.0 μg/mL). This finding indicated that a providential lipophilic group located at *N*-position could enhance bioactivity. By contrast, the pharmaceutical effect was decreased due to the fused 4-fluorobenzyl group (**B_5**, 11.8%, 50 μg/mL). Thus, a sterically hindered substitute at this location could restrict further coactions with tested bacteria. The anti-*Xac* activity potency was considerably elevated after C_1–C_4 alkyl groups were introduced, which revealed that a relative lipophilic group at this location could promote pharmacological activity. However, a substituted group with

small steric hindrance was preferred for the anti-*Xac* activity and resulted in the minimal EC_{50} value of 19.9 μg/mL for **B_1** with a methyl group. Similar patterns were observed for **B_5** (4-fluorobenzyl, 11.6%, 100 μg/mL) due to a large sterically hindered moiety that provided negligible growth inhibition effects against *Xac*. On the basis of the above results, ameliorative antibacterial efficiency was achieved by the rational design and renovation of molecular structures.

Given that **A_1**, **B_1**, and **B_2** with NH, NCH_3, and NCH_2CH_3 patterns, respectively, had excellent potential as antibacterial indicators, the bioactivity of the substituents on the quinazoline ring was investigated (Figure 4). To test the type of halogen atom with bioactivity, **C_1**, **D_1**, and **E_1** with a Cl atom instead of Br atom were initially prepared, and their antibacterial effects were investigated (Table 3). A slightly improved potency against *Xoo* was observed by comparing the EC_{50} values of **A_1** (6-Br, 9.77 μg/mL) and **C_1** (6-Cl, 7.13 μg/mL), **B_1** (6-Br, 14.1 μg/mL) and **D_1** (6-Cl, 12.7 μg/mL). **E_1** (6-Cl, 12.1 μg/mL) had a reduced bioactivity compared with that of **B_2** (6-Br, 7.03 μg/mL). Of note, the anti-*Xac* efficacies of **C_1**, **D_1**, and **E_1** were considerably increased via the switching of -Br with -Cl, and EC_{50} values of 18.6, 17.9, and 15.6 μg/mL were obtained, respectively. Subsequently, the effects of substituent position on the quinazoline ring on bioactivity were investigated. Cl atom at 6-, 5-, 7-, or 8-position had different effects on antibacterial action. Particularly, 6-Cl on the quinazoline ring had the strongest biological activity against *Xoo* compared with those of **C_1–C_4**, **D_1–D_4**, and **E_1–E_4**. The antibiotic properties of **C_3** and **D_4** with the relevant 7-Cl and 8-Cl motifs were completely quenched, suggesting that

even small structural variations could prominently influence the final biological functions. As such, the molecular architectures should be deliberately optimized. For anti-*Xac* activity, the Cl atom at 5- or 6-position showed acceptable inhibition effects, whereas **C$_3$**, **E$_3$**, **C$_4$**, and **D$_4$** with 7-Cl or 8-Cl patterns had negligible inhibition rates of < 50% at 100 μg/mL. Among these analogues, **E$_4$** with 8-Cl and *N*-CH_2CH_3 motifs had the best anti-*Xac* capacity with the lowest EC_{50} value of 10.3 μg/mL. In view of the above analysis, the electronic property of substituents on the quinazoline ring and its effects on bioactivity were studied. After the weak electron-withdrawing group (i.e., 6-Br or 6-Cl) was removed from the structure, series **A$_1$** (6-Br, 9.77 μg/mL) and **C$_1$** (6-Cl, 7.13 μg/mL) was compared. **C$_5$** (H, 24.1 μg/mL) had decreased anti-*Xoo* activity, whereas **D$_5$** (H, 10.1 μg/mL) had a slightly improved potency compared with **B$_1$** (6-Br, 14.1 μg/mL) and **D$_1$** (6-Cl, 12.7 μg/mL). Changing 6-Br or 6-Cl into a weak electron-donating group (6-CH_3) resulted in considerable anti-*Xoo* activity of **C$_6$**, **D$_6$**, and **E$_6$** with EC_{50} values of 7.24–8.75 μg/mL, which were comparable with those of **C$_1$** (6-Cl, NH, 7.13 μg/mL) and **B$_2$** (6-Br, NCH_2CH_3, 7.03 μg/mL). The anti-*Xac* activity of compounds substituted with H or 6-CH_3 had EC_{50} values of 14.6–39.0 μg/mL. Surprisingly, the antibacterial efficiency against the two strains was significantly decreased by introducing the strong electron-donating group of 6,7-diOCH_3 moiety. Thus, this kind of substitutional groups could severely block interactions with target species. Given the above results, **B$_2$** (6-Br, NCH_2CH_3, 7.03 μg/mL) and **C$_1$** (6-Cl, NH, 7.13 μg/mL) with the greatest antibacterial effects against *Xoo* were chosen for further *in vivo* research.

To determine the prospective application, *in vivo* trials against rice bacterial blight were performed. As shown in Table 4 and Figure 5, the highly active compounds **B_2** and **C_1** presented excellent *in vivo* curative behavior with corresponding efficacy of 51.55% and 49.02% at 200 μg/mL, respectively. Their protective effects were also remarkable with relevant control rates of 49.84% and 52.17%, which were also superior to **BT** (40.23%) and **TC** (39.29%). This finding indicated that the designed compounds should be explored and developed as alternatives in antibacterial chemotherapy.

To elucidate the possible antibacterial mechanism of target compounds, quantitative proteomic assay should be performed via treatment of *Xoo* with **C_1**. Clearly, 2342 proteins have been preliminary monitored for the control and treatment samples (three repetitions). The related protein quantitative repeatability was assessed using relative standard deviation assay (Figure 6a). Notably, 2078 proteins (88.7%) were the common assets for the two groups (**C_1** and **CK**) and contained the quantitative information (Table S1). Comparative proteomic identification (**C_1/CK**) demonstrated that 292 proteins had been differentially expressed, among which 159 proteins and 133 proteins were up-regulated and down-regulated, respectively (fold changes > 1.5, Table S2 and Figures 6b and 6c). To further explain their biological functions, these proteins have been processed for GO categories in BP, CC, and MF.[53,54] As shown in Figure 7a, these proteins were mainly related to metabolic and cellular processes, localization, biological regulation, locomotion, signaling, and cellular component organization or biogenesis. CC analysis (Figure 7b) showed that a

346 mass of differentially expressed proteins were localized in the membrane, cell,
347 organelle, and macromolecular complex. Figure 7c showed that those proteins
348 participated in catalytic activity, binding, molecular and signal transducer activities,
349 structural molecule activity, and transporter activity. Moreover, the subcellular
350 structure location pattern (Figure Sa) suggested that a great deal of those proteins
351 were located in bacterial cytoplasm. Thus, the designed compound **C_1** had the most
352 significant ability to affect the physiological process of pathogens.

353 To further classify and predict the possible functions of these unique proteins, the
354 Clusters of Orthologous Groups (COG) analysis was employed for functional
355 classification statistics. In this section, 238 proteins were assigned to COG
356 classifications (Figure Sb), and consequently afforded 20 functional categories
357 including "General function prediction only," "Carbohydrate transport and
358 metabolism," "Function unknown," "Amino acid transport and metabolism,"
359 "Translation," "ribosomal structure and biogenesis," "Lipid transport and
360 metabolism," "Energy production and conversion," "Transcription," and "Coenzyme
361 transport and metabolism". This finding suggested that **C_1** probably played a crucial
362 role in regulating late-stage energy metabolism.[55]

363 To elucidate the possible action pathways triggered by **C_1**, the KEGG pathway
364 map was used to determine the relevant pathways involved in these differentially
365 expressed proteins. As a result, we enriched two pathways including sucrose and
366 starch metabolism and biotin metabolism (Figure Sc).[56-58] As far as we know, the
367 sucrose and starch metabolic pathway can provide energy and carbon sources to the

368 living body through the glycolysis process,[59,60] while the biotin metabolism pathway
369 plays a significant role in fatty acid metabolism, sugar metabolism, amino acid
370 metabolism, and protein synthesis, ultimately affecting energy metabolism of the
371 life.[61,62] The two detailed pathways were illustrated in Figure 8, which revealed that
372 the biosynthesis of D-glucose and biotin was significantly affected by these variably
373 expressed proteins stimulated from $\mathbf{C_1}$. In the D-glucose metabolic pathway, various
374 prominent proteins were upregulated, such as endoglucanase, trehalose-6-phosphate
375 synthase, cellulose 1,4-beta-cellobiosidase, and trehalose 6-phosphate phosphatase,
376 whereas beta-glucosidase (bglu, EC 3.2.1.21) and periplasmic trehalase (treA, EC
377 3.2.1.28) were downregulated at the last biosynthesis of D-glucose. This observed
378 result further confirmed that the biosynthesis of D-glucose was strongly disturbed. For
379 example, one of the effective routes for D-glucose synthesis was that the up-regulated
380 otsA could facilitate the condensation of UDP-glucose and glucose-6-phosphate to
381 create trehalose-6-phosphate along with the removal of UDP; subsequently, the
382 up-regulated otsB would promote the hydrolysis of trehalose-6-phosphate to form
383 trehalose; however, in the final step, the down-regulated treA could dramatically
384 prevent the normal decomposition of trehalose into D-glucose, which consequently
385 resulted in the blockage of this synthetic route and the final shortage of D-glucose. In
386 biotin metabolic pathway, the upregulated proteins, including malonyl-[acp]
387 o-methyltransferase and pimeloyl-[acp] methyl ester esterase, would greatly influence
388 the key biosynthesis of intermediate metabolites of malonyl-[acp] methyl ester and
389 pimeloyl-[acp]. Meanwhile, downregulated proteins, including 3-oxoacyl-[acp]

reductase, 8-amino-7-oxononanoate synthase, ATP-dependent dethiobiotin synthetase, and biotin synthase, were observable, which probably resulted in the biosynthetic reduction of biotin. These results demonstrated that **C_1** might possess the privileged competence to regulate and disrupt the pathways of synthesis of D-glucose and biotin, which subsequently affected the energy metabolism in *Xoo* and consequently led to the bacterial death.

To understand the association of these differentially expressed proteins, protein–protein interaction networks should be generated by using STRING database version 10.5.[49] In this section, we screened out the top strongly interacted 50 differentially expressed proteins to make the interacting network analysis. As shown in Figure 9, the "glucose metabolizing enzyme" referring to the sucrose and starch metabolic pathway and the "biotin synthase" associated with the biotin metabolic pathway were significantly enriched. Moreover, other sub-networks were identified and enriched, including "citrate synthase," "flagellar motor protein," "tryptophan halogenase," "Fe/S biogenesis protein," "secretion protein," "transcriptional regulator," "RNA polymerase," "galactosidase," "Acyl-CoA dehydrogenase," and "phosphate reductase". This result suggested that a portion of these differentially expressed proteins which could be triggered and regulated by **C_1** stimulation had significant roles in various physiological processes.

In order to further prove the final and substantial levels of these differentially expressed proteins involved in D-glucose and biotin pathways, two approaches are usually used which are detection of transcription levels of some representative genes

412 and parallel reaction monitoring (PRM). Considered that transcript levels are only a
413 moderate predictor for protein expression,[63,64] PRM technique that is capable of
414 accurately quantifying various target proteins, was performed.[65,66] In this experiment,
415 19 significant differentially expressed proteins from D-glucose metabolic pathway,
416 biotin metabolic pathway and GO terms were chosen for PRM assay. Simultaneously,
417 two specialized peptides for each tested protein were selected for the quantitative
418 analysis (Tables S3-4). Clearly, the obtained PRM data displayed the similar tendency
419 with the above-motioned quantitative proteomics result (Figure 10), further
420 confirming **C_1** could affect the biosynthesis of D-glucose and biotin pathways.

421 To study the variation on the morphology and integrity of pathogens after
422 treatment with designed compounds, SEM images were provided via a concentration
423 dependent manner. **C_1** (7.13 μg/mL) and **E_4** (10.3 μg/mL) against the corresponding
424 *Xoo* and *Xac* were selected for these detections. The pathogen morphology and
425 integrity of pathogens were significantly affected by the drug concentration. At the
426 drug dose of 50 μg/mL, unequally shaped, partially corrugated, or broken
427 morphologies (Figures 11b, 11c, 11f, and 11g) were observed compared with those of
428 *Xoo* or *Xac* without drug treatment (Figures 11a and 11e). Further increasing the dose
429 to 100 μg/mL caused the emergence of large leakage holes and fragmentary bacteria
430 (Figures 11d and 11h). This result was in accordance with the gradually elevated
431 fluorescent intensity at 600 nm (Figure 12) with different drug concentrations, in
432 which the newly produced fluorescence was caused by the formation of PI-DNA
433 complex.[51] This finding suggested that **C_1** and **E_4** could change and promote the

membrane permeability. Given the above results, this type of designed compounds had strong interactions targeting tested pathogens, thereby causing the changes and disturbances on their physiological process and finally bacterial death.

In summary, a series of simple furan-functionalized quinazolin-4-amines was systematically prepared and screened their antimicrobial activity. Results displayed that **C_1** and **E_4** exhibited excellent competences for suppressing the growth of pathogens *Xoo* and *Xac*, displaying the corresponding EC_{50} values of 7.13 and 10.3 μg/mL. *In vivo* study further identified the promising application against bacterial infections. Quantitative proteomic bioassay demonstrated that **C_1** could dramatically induce the upregulation and downregulation of an array of expressed proteins which probably involved in D-glucose and biotin metabolic pathways. This outcome was further confirmed by PRM analysis. Concentration-dependent SEM images and fluorescence spectra indicated that the designed compounds had the versatile capacity for destroying the integrity of bacteria and increasing membrane permeability. Given the simple molecular skeleton, easily prepared procedures, and highly efficient bioactivity, we recommend that this kind of molecular architecture should be developed as a novel lead indicator in the chemotherapeutic field of bacterial diseases.

Acknowledgment

We acknowledge China's funds from NNSF (21877021, 31860516, 21702037, 21662009), Research Project of Ministry of Education (213033A, 20135201110005), and Guizhou PSTP ([2017]5788, LH [2017]7259, [2012]6012).

Supporting Information

Supporting information including Experimental procedures for PRM, Tables S1-S4, Figures Sa-Sc, Preparation and characterization data of title compounds, NMR and HRMS spectra of $\mathbf{A_1}$-$\mathbf{A_7}$, $\mathbf{B_1}$-$\mathbf{B_5}$, $\mathbf{C_1}$-$\mathbf{C_7}$, $\mathbf{D_1}$-$\mathbf{D_7}$, $\mathbf{E_1}$-$\mathbf{E_7}$ (Figure S1 to S101) associated with this article can be found, in the online version, at https://pubs.acs.org/journal/jafcau.

Conflict of interest

The authors declare no competing financial interest.

References

(1) Friedman, M. Antibiotic-resistant bacteria: prevalence in food and inactivation by food-compatible compounds and plant extracts. *J. Agric. Food Chem.* **2015**, *63*, 3805-3822.

(2) Badawy, M. E. I.; Abdelgaleil, S. A. M. Composition and antimicrobial activity of essential oils isolated from Egyptian plants against plant pathogenic bacteria and fungi. *Ind. Crop. Prod.* **2014**, *52*, 776-782.

(3) Friedman, M. Chemistry, antimicrobial mechanisms, and antibiotic activities of cinnamaldehyde against pathogenic bacteria in animal feeds and human foods. *J. Agric. Food Chem.* **2017**, *65*, 10406-10423.

(4) Li, B.; Liu, B.; Shan, C.; Ibrahim, M.; Lou, Y.; Wang, Y.; Xie, G.; Li, H. Y.; Sun, G. Antibacterial activity of two chitosan solutions and their effect on rice bacterial leaf blight and leaf streak. *Pest Manag. Sci.* **2013**, *69*, 312-320.

(5) Zheng, Y. T.; Zhang, T. T.; Wang, P. Y.; Wu, Z. B.; Zhou, L.; Ye, Y. Q.; Zhou, X.; He, M.; Yang, S. Synthesis and bioactivities of novel 2-(thioether/sulfone)-5-pyrazolyl-1,3,4-oxadiazole derivatives. *Chin. Chem. Lett.* **2017**, *28*, 253-256.

(6) Li, P.; Hu, D. Y.; Xie, D. D.; Chen, J. X.; Jin, L. H.; Song, B. A. Design, Synthesis, and evaluation of new sulfone derivatives containing a 1,3,4-oxadiazole moiety as active antibacterial agents. *J. Agric. Food Chem.* **2018**, *66*, 3093-3100.

(7) Zhang, A. J.; Hartung, J. S. Phenylacetaldehyde O-methyloxime: a volatile

compound produced by grapefruit leaves infected with the citrus canker pathogen, *xanthomonas axonopodis* pv. *citri.*. *J. Agric. Food Chem.* **2005**, *53*, 5134-5137.

(8) Zhang, S. J.; Wang, L.; Zhao, R. R.; Yu, W. Q.; Li, R.; Li, Y. J.; Sheng, J. Q.; Shen, L. Knockout of SIMAPK3 reduced disease resistance to *botrytis cinerea* in tomato plants. *J. Agric. Food Chem.* **2018**, *66*, 8949-8956.

(9) Li, P.; Shi, L.; Yang, X.; Yang, L.; Chen, X. W.; Wu, F.; Shi, Q. C.; Xu, W. M.; He, M.; Hu, D. Y.; Song, B. A. Design, synthesis, and antibacterial activity against rice bacterial leaf blight and leaf streak of 2,5-substituted-1,3,4-oxadiazole/thiadiazole sulfone derivative. *Bioorg. Med. Chem. Lett.* **2014**, *24*, 1677-80.

(10) Choi, C.; Park, S.; Ahn, I.; Bae, S.; Hwang, D. Generation of Chinese cabbage resistant to bacterial soft rot by heterologous expression of arabidopsis WRKY75. *Plant Biotechnol. Rep.* **2016**, *10*, 301-307.

(11) He, K.; Yang, S. Y.; Li, H.; Wang, H.; Li, Z. L. Effects of calcium carbonate on the survival of *Ralstonia solanacearum* in soil and control of tobacco bacterial wilt. *Eur. J. Plant Pathol.* **2014**, *140*, 665-675.

(12) Hasegawa, T.; Kato, Y.; Okabe, A.; Itoi, C.; Ooshiro, A.; Kawaide, H.; Natsume, M. Effect of secondary metabolites of tomato (*Solanum lycopersicum*) on chemotaxis of *ralstonia solanacearum*, pathogen of bacterial wilt disease. *J. Agric. Food Chem.* **2019**, *67*, 1807-1813.

(13) Qiao, M.; Ying, G. G.; Singer, A. C.; Zhu, Y. G. Review of antibiotic resistance

508 in China and its environment. *Environ. Int.* **2018**, *110*, 160-172.

509 (14) Buttimer, C.; Mukhtar, O.; Ross, R. P.; Hill, C.; O'Mahony, J.; Coffey, A.
510 Bacteriophages and bacterial plant diseases. *Front. Microbiol.* **2017**, *8*.10-15.

511 (15) Wang, P. Y.; Fang, H. S.; Shao, W. B.; Zhou, J.; Chen, Z.; Song, B. A.; Yang, S.
512 Synthesis and biological evaluation of pyridinium-functionalized carbazole
513 derivatives as promising antibacterial agents. *Bioorg. Med. Chem. Lett*. **2017**, *27*,
514 4294-4297.

515 (16) Aslam, M. N.; Mukhtar, T.; Ashfaq, M.; Hussain, M. A. Evaluation of chili
516 germplasm for resistance to bacterial wilt caused by *Ralstonia solanacearum*.
517 *Australas. Plant Path.* **2017**, *46*, 289-292.

518 (17) Li, J.; Zhou, M. G.; Li, H. X.; Chen, C. J.; Wang, J. X.; Zhang, Y. J. A study on
519 the molecular mechanism of resistance to amicarthiazol in *xanthomonas*
520 *campestris* pv. *citri.*. *Pest Manag. Sci.* **2006**, *62*, 440-445.

521 (18) Xu, W. M.; Li, S. Z.; He, M.; Yang, S.; Li, X. Y.; Li, P. Synthesis and
522 bioactivities of novel thioether/sulfone derivatives containing 1,2,3-thiadiazole
523 and 1,3,4-oxadiazole/thiadiazole moiety. *Bioorg. Med. Chem. Lett.* **2013**, *23*,
524 5821-5824.

525 (19) Liang, X.; Duan, Y.; Yu, X.; Wang, J.; Zhou, M. Photochemical degradation of
526 bismerthiazol: structural characterisation of the photoproducts and their inhibitory
527 activities against *Xanthomonas oryzae pv. oryzae*. *Pest Manag. Sci.* **2016**, *72*,
528 997-1003.

529 (20) Xin, M.; Duan, W.; Feng, Y.; Hei, Y. Y.; Zhang, H.; Shen, Y.; Zhao, H. Y.; Mao,

S.; Zhang, S. Q. Novel 6-aryl substituted 4-pyrrolidineaminoquinazoline derivatives as potent phosphoinositide 3-kinase delta (PI3Kdelta) inhibitors. *Bioorg. Med. Chem.* **2018**, *26*, 2028-2040.

(21) Chen, Y. C.; Backus, K. M.; Merkulova, M.; Yang, C.; Brown, D.; Cravatt, B. F.; Zhang, C. Covalent modulators of the vacuolar ATPase. *J. Am. Chem. Soc.* **2017**, *139*, 639-642.

(22) Zeng, M.; Lu, J.; Li, L.; Feru, F.; Quan, C.; Gero, T. W.; Ficarro, S. B.; Xiong, Y.; Ambrogio, C.; Paranal, R. M.; Catalano, M.; Shao, J.; Wong, K. K.; Marto, J. A.; Fischer, E. S.; Janne, P. A.; Scott, D. A.; Westover, K. D.; Gray, N. S. Potent and selective covalent quinazoline inhibitors of KRAS G12C. *Cell Chem. Biol.* **2017**, *24*, 1005-1016.

(23) Parhi, A. K.; Zhang, Y. Z.; Saionz, K. W.; Pradhan, P.; Kaul, M.; Trivedi, K.; Pilch, D. S.; LaVoie, E. J. Antibacterial activity of quinoxalines, quinazolines, and 1,5-naphthyridines. *Bioorg. Med. Chem. Lett.* **2013**, *23*, 4968-4974.

(24) Fleeman, R.; Van Horn, K. S.; Barber, M. M.; Burda, W. N.; Flanigan, D. L.; Manetsch, R.; Shaw, L. N. Characterizing the antimicrobial activity of N^2, N^4-disubstituted quinazoline-2,4-diamines toward multidrug-resistant acinetobacter baumannii. *Antimicrob. Agents Chemother* **2017**, *61*, e00059-17.

(25) Alafeefy, A. M.; Kadi, A. A.; Al-Deeb, O. A.; El-Tahir, K. E. H.; Al-jaber, N. A. Synthesis, analgesic and anti-inflammatory evaluation of some novel quinazoline derivatives. *Eur. J. Med. Chem.* **2010**, *45*, 4947-4952.

(26) Kang, D.; Zhang, H.; Zhou, Z.; Huang, B.; Naesens, L.; Zhan, P.; Liu, X. First

552 discovery of novel 3-hydroxy-quinazoline-2,4(1*H*,3*H*)-diones as specific
553 anti-vaccinia and adenovirus agents via 'privileged scaffold' refining approach.
554 *Bioorg. Med. Chem. Lett.* **2016**, *26*, 5182-5186.
555 (27) El-Gazzar, A. B. A.; Youssef, M. M.; Youssef, A. M. S.; Abu-Hashem, A. A.;
556 Badria, F. A. Design and synthesis of azolopyrimidoquinolines,
557 pyrimidoquinazolines as anti-oxidant, anti-inflammatory and analgesic activities.
558 *Eur. J. Med. Chem.* **2009**, *44*, 609-624.
559 (28) Guan, J.; O'Neil, M.; Obaldia, N.; Ager, A.; Gerena, L.; Lin, A. J. Antimalarial
560 activities of new pyrrolo[3,2-f]quinazoline-1,3-diamine derivatives. *Antimicrob.*
561 *Agents Chemother* **2005**, *49*, 4928-4933.
562 (29) Ali, Z.; Akhtar, M. J.; Siddiqui, A. A.; Khan, A. A.; Haider, M. R.; Yar, M. S.
563 Design, synthesis, and biological evaluation of novel quinazoline clubbed
564 thiazoline derivatives. *Arch. Pharm. Chem. Life Sci.* **2017**, *350*, 349-352.
565 (30) Mujeeb Ur, R.; Rathore, A.; Siddiqui, A. A.; Parveen, G.; Yar, M. S. Synthesis
566 and characterization of quinazoline derivatives: search for hybrid molecule as
567 diuretic and antihypertensive agents. *J. Enzyme Inhib. Med. Chem.* **2014**, *29*,
568 733-743.
569 (31) Maemondo, M.; Inoue, A.; Kobayashi, K.; Sugawara, S.; Oizumi, S.; Isobe, H.;
570 Gemma, A.; Harada, M.; Yoshizawa, H.; Kinoshita, I.; Fujita, Y.; Okinaga, S.;
571 Hirano, H.; Yoshimori, K.; Harada, T.; Ogura, T.; Ando, M.; Miyazawa, H.;
572 Tanaka, T.; Saijo, Y.; Hagiwara, K.; Morita, S.; Nukiwa, T. Gefitinib or
573 chemotherapy for non–small cell lung cancer with mutated EGFR. *N. Engl. J.*

574 *Med.* **2010**, *362*, 2380-2388.

575 (32) Perez-Soler, R.; Chachoua, A.; Hammond, L. A.; Rowinsky, E. K.; Huberman,
576 M.; Karp, D.; Rigas, J.; Clark, G. M.; Santabarbara, P.; Bonomi, P. Determinants
577 of tumor response and survival with erlotinib in patients with non-small-cell lung
578 cancer. *J. Clin. Oncol.* **2004**, *22*, 3238-3247.

579 (33) Trinks, C.; Severinsson, E. A.; Holmlund, B.; Green, A.; Green, H.; Jonsson, J. I.;
580 Hallbeck, A. L.; Walz, T. M. The pan-ErbB tyrosine kinase inhibitor canertinib
581 induces caspase-mediated cell death in human T-cell leukemia (Jurkat) cells.
582 *Biochem. Biophys. Res. Commun.* **2011**, *410*, 422-427.

583 (34) Snyder, R. D.; Boyle, F. M.; Chan, A.; Craft, P. S.; Boer, R. D. E.; Mainwaring,
584 P. N.; McCarthy, N. J.; Wilcken, N. R. Clinical recommendations for the use of
585 lapatinib ditosylate plus capecitabine for patients with advanced or metastatic
586 HER2-positive breast cancer. *Asia-Pac. J. Clin. Onco.* **2009**, *5*, 4-16.

587 (35) Dawson, W. A. J. M.; Bateman, G. L. Fungal communities on roots of wheat and
588 barley and effects of seed treatments containing fluquinconazole applied to
589 control take-all. *Plant Pathol.* **2001**, *50*, 75-82.

590 (36) Solomon, M. G.; Fitzgerald, J. D.; Ridout, M. S. Fenazaquin, a selective acaricide
591 for use in IPM in apple in the UK. *Crop Prot.* ***1*999**, *12*, 255-258.

592 (37) Yasunaga, R.; Ikuta, J.; Murata, Y.; Inoue, K.; Koga, H.; Masaki, T.; Tamura, H.
593 Ligand-independent androgen receptor antagonism caused by the newly
594 developed pesticide pyrifluquinazon (PFQ). *Reprod. Toxicol.* **2013**, *35*, 1-6.

595 (38) Van Horn, K. S.; Burda, W. N.; Fleeman, R.; Shaw, L. N.; Manetsch, R.

Antibacterial activity of a series of N^2, N^4-disubstituted quinazoline-2,4-diamines. *J. Med. Chem.* **2014**, *57*, 3075-3093.

(39) Gotrasova, R.; Kubfkova, J.; Qipak, E. Antibacterial effect of some 2,6-disubstituted 4-anilinoquinazolines. *Folia Microbio.* **1998**, *43*, 679-682.

(40) Chandrika, P. M.; Yakaiah, T.; Narsaiah, B.; Sridhar, V.; Venugopal, G.; Rao, J. V.; Kumar, K. P.; Murthy, U. S. N.; Rao, A. R. R. Synthesis leading to novel 2,4,6-trisubstituted quinazoline derivatives, their antibacterial and cytotoxic activity against THP-1, HL-60 and A375 cell lines. *Indian J. Chem.* **2009**, *48*, 840-847.

(41) Wang, X. D.; Wei, W.; Wang, P. F.; Tang, Y. T.; Deng, R. C.; Li, B.; Zhou, S. S.; Zhang, J. W.; Zhang, L.; Xiao, Z. P.; Ouyang, H.; Zhu, H. L. Novel 3-arylfuran-2(*5H*)-one-fluoroquinolone hybrid: Design, synthesis and evaluation as antibacterial agent. *Bioorg. Med. Chem.* **2014**, *22*, 3620-3628.

(42) Alnabulsi, S.; Hussein, B.; Santina, E.; Alsalahat, I.; Kadirvel, M.; Magwaza, R. N.; Bryce, R. A.; Schwalbe, C. H.; Baldwin, A. G.; Russo, I.; Stratford, I. J.; Freeman, S. Evaluation of analogues of furan-amidines as inhibitors of NQO2. *Bioorg. Med. Chem. Lett.* **2018**, *28*, 1292-1297.

(43) Aslam, S. N.; Stevenson, P. C.; Kokubun, T.; Hall, D. R. Antibacterial and antifungal activity of cicerfuran and related 2-arylbenzofurans and stilbenes. *Microbiol. Res.* **2009**, *164*, 191-195.

(44) Wen, F.; Jin, H.; Tao, K.; Hou, T. Design, synthesis and antifungal activity of novel furancarboxamide derivatives. *Eur. J. Med. Chem.* **2016**, *120*, 244-251.

618 (45) Nageshwara, R. C.; Blessi, P. K.; Ravi, J.; Kusuma, B. K. T.; Gade, D. Synthesis
619 and antimicrobial evaluation of 2-(aialkylamino)-N-(5-(5-alkylthio)
620 -1,3,4-ocadiazol-2-yl)benzoxazol-2-yl)acetamides. *J. Int. Pharm. Res.* **2014**, *3*,
621 387-397.
622 (46) Junshi, M. Degradation, metabolism and toxicity of synthetic pyrethroids.
623 *Environ. Health Persp.* **1976**, *14*, 15-28.
624 (47) Sandmann, G.; Ward, C. E.; Lo, W. C.; Nagy, J. O.; Boger, P. Bleaching
625 herbicide flurtamone interferes with phytoene desaturase. *Plant Physiol*. **1990**,
626 *94*, 476-478.
627 (48) Chen, J.; Shi, J.; Yu, L.; Liu, D. Y.; Gan, X. H.; Song, B. A.; Hu, D. Y. Design,
628 synthesis, antiviral bioactivity, and defense mechanisms of novel dithioacetal
629 derivatives bearing a strobilurin moiety. *J. Agric. Food Chem.* **2018**, *66*,
630 5335-5345.
631 (49) Chen, X. L.; Xie, X.; Wu, L. Y.; Liu, C. Y.; Zeng, L. R.; Zhou, X. P.; Luo, F.;
632 Wang, G. L.; Liu, W. D. Proteomic analysis of ubiquitinated proteins in rice
633 (*Oryza sativa*) after treatment with pathogen-associated molecular pattern
634 (PAMP) elicitors. *Front. Plant Sci.* **2018**, *9*, 1064.
635 (50) He, D.; Wang, Q.; Li, M.; Damaris, R. N.; Yi, X.; Cheng, Z.; Yang, P. Global
636 proteome analyses of lysine acetylation and succinylation reveal the widespread
637 involvement of both modification in metabolism in the embryo of germinating
638 rice seed. *J. Proteome Res.* **2016**, *15*, 879-890.
639 (51) Zhou, J.; Tao, Q. Q.; Wang, P. Y.; Shao, W. B.; Wu, Z. B.; Li, Z.; Yang, S.

Antimicrobial evaluation and action mechanism of pyridinium-decorated 1,4-pentadien-3-one derivatives. *Bioorg. Med. Chem. Lett.* **2018**, *28*, 1742-1746.

(52) Zhang, Y.; Jin, L. H.; Xiang, H. M.; Wu, J.; Wang, P. Y.; Hu, D. Y.; Xue, W.; Yang, S. Synthesis and anticancer activities of 5,6,7-trimethoxy-N-phenyl(ethyl) -4-aminoquinazoline derivatives. *Eur. J. Med. Chem.* **2013**, *66*, 335-344.

(53) Shi, J.; Yu, L.; Song, B. A. Proteomics analysis of xiangcaoliusuobingmi-treated *capsicum annuum L.* infected with *cucumber mosaic virus*. *Pestic. Biochem. Phys.* **2018**, *149*, 113-122.

(54) Song, X. P.; Li, P.; Li, M. W.; Yang, A. M.; Yu, L.; Luo, L. G.; Hu, D. Y.; Song, B. A. Synthesis and investigation of the antibacterial activity and action mechanism of 1,3,4-oxadiazole thioether derivatives. *Pestic. Biochem. Phys.* **2018**, *147*, 11-19.

(55) Madda, R.; Lin, S. C.; Sun, W. H.; Huang, S. L. Plasma proteomic analysis of systemic lupus erythematosus patients using liquid chromatography/tandem mass spectrometry with label-free quantification. *Peer J.* **2018**, *6*, e4730.

(56) Gao, M. P.; Zhang, S. W.; Luo, C.; He, X. H.; Wei, S. L.; Jiang, W.; He, F. L.; Lin, Z. C.; Yan, M. X.; Dong, W. Q. Transcriptome analysis of starch and sucrose metabolism across bulb development in *Sagittaria sagittifolia*. *Gene* **2018**, *649*, 99-112.

(57) Leon, D. R. A. Biotin in metabolism, gene expression and human disease. *J. Inherit. Metab. Dis.* **2019**, doi: 10.1002/jimd.12073.

(58) Kumar, R.; Mukherjee, S.; Ayele, B. T. Molecular aspects of sucrose transport

662 and its metabolism to starch during seed development in wheat: a comprehensive
663 review. *Biotechnol. Adv.* **2018**, *36*, 954-967.
664 (59) Zhang, L.; Lin Q.; Feng, Y. Z.; Fan, X. M.; Zou, F.; Yuan, D. Y.; Zeng, X. C.;
665 Cao, H. P. Transcriptomic identification and expression of starch and sucrose
666 metabolism genes in the seeds of Chinese chestnut (*Castanea mollissima*). *J.*
667 *Agric. Food Chem.* **2015**, *63*, 929-942.
668 (60) Piazza, A.; Zimaro, T.; Garavaglia, B. S.; Ficarra, F. A.; Thomas, L.;
669 Marondedze, C.; Feil, R.; Lunn, J. E.; Gehring, C.; Ottado, J.; Gottig, N. The dual
670 nature of trehalose in citrus canker disease: a virulence factor for *Xanthomonas*
671 *citri subsp. citri* and a trigger for plant defence responses. *J. Exp. Bot.* **2015**, *66*,
672 2795-2811.
673 (61) Diana, P. A. R.; Sergio, S. V.; Alfonso, L. D. R. Biotin in metabolism and its
674 relationship to human disease. *Arch. Med. Res.* **2002**, *33*, 439-447.
675 (62) Li, J.; Brader, G.; Helenius, E.; Kariola, T.; Palva, E. T. Biotin deficiency causes
676 spontaneous cell death and activation of defense signaling. *Plant J.* **2012**, *70*,
677 315-326.
678 (63) Liu,Y.; Beyer, A.; Aebersold, R. On the dependency of cellular protein levels on
679 mRNA abundance. *Cell* **2016**, *165*, 535–550.
680 (64) Vogel, C.; Marcotte, E. M. Insights into the regulation of protein abundance from
681 proteomic and transcriptomic analyses. *Nat. Rev. Genet.* **2012**, *13*, 227–232.
682 (65) Rauniyar, N. Parallel reaction monitoring: a targeted experiment performed using
683 high resolution and high mass accuracy mass spectrometry. *Int. J. Mol. Sci*. **2015**,

16, 28566-28581.

(66) Zhao, Y. L.; Huang, X.; Liu, L. W.; Wang, P. Y.; Long, Q. S.; Tao, Q. Q.; Li, Z.; Yang, S. Identification of racemic and chiral carbazole derivatives containing an isopropanolamine linker as prospective surrogates against plant pathogenic bacteria: in vitro and in vivo assays and quantitative proteomics. *J. Agric. Food Chem.* **2019**, *67*, 7512-7525.

690 **Figure captions**

691 **Figure 1.** a) Some of the discovered bioactive frameworks possessing quinazoline or
692 furan scaffolds. b) Design strategy for title compounds.

693 **Figure 2.** Synthesis for title compounds $\mathbf{A_1}$–$\mathbf{A_7}$.

694 **Figure 3.** Synthesis for title compounds $\mathbf{B_1}$–$\mathbf{B_5}$.

695 **Figure 4.** Synthesis for title compounds $\mathbf{C_1}$–$\mathbf{C_7}$, $\mathbf{D_1}$–$\mathbf{D_7}$, and $\mathbf{E_1}$–$\mathbf{E_7}$.

696 **Figure 5.** *In vivo* control efficacy' images of $\mathbf{B_2}$ and $\mathbf{C_1}$ against rice bacterial blight;
697 **BT** and **TC** were the positive controls at the same conditions.

698 **Figure 6.** a) RSD analysis of three repetitions. b) Histogram of the number
699 distribution of differentially expressed proteins in different comparison groups
700 ($\mathbf{C_1}$/**CK**). c) Volcano plot of differentially expressed proteins ($\mathbf{C_1}$/**CK**).

701 **Figure 7.** GO analysis expressed in (a) BP, (b) CC, and (c) MF.

702 **Figure 8.** Schematic of D-glucose and biotin metabolic pathways. Red and green
703 indicate the corresponding upregulated and downregulated proteins.

704 **Figure 9.** Protein-protein interaction networks for differentially expressed proteins.
705 The circles indicate differentially expressed proteins, and blue and red represent the
706 corresponding downregulated and upregulated proteins.

707 **Figure 10.** PRM analysis for 19 selected differentially expressed proteins.

708 **Figure 11.** SEM patterns of *Xoo* after incubation in various dosages of $\mathbf{C_1}$, (a) 0, (b, c)
709 50, and (d) 100 μg/mL. SEM patterns of *Xac* after incubation in various dosages of $\mathbf{E_4}$,
710 (e) 0, (f, g) 50, and (h) 100 μg/mL. Scale bars for (a–h) are 1 μm.

711 **Figure 12.** Fluorescent intensities stained with PI for the solution containing (a) *Xoo*

712 or (b) *Xac* after incubation with various dosages of $\mathbf{C_1}$ and $\mathbf{E_4}$, respectively.

713

Tables

Table 1. Preliminary antibacterial assays of target molecules $\mathbf{A_1}$–$\mathbf{A_7}$ toward pathogens *Xoo* and *Xac in vitro*.

Compounds	*Xoo*		*Xac*	
	Inhibition ratio (%)		Inhibition ratio (%)	
	50 μg/mL	25 μg/mL	100 μg/mL	50 μg/mL
$\mathbf{A_1}$	100	100	43.8±3.0	25.7±2.1
$\mathbf{A_2}$	0	0	41.2±2.6	0
$\mathbf{A_3}$	0	0	18.5±3.7	0
$\mathbf{A_4}$	0	0	22.4±0.5	0
$\mathbf{A_5}$	40.0±3.5	20.2±1.4	15.3±2.0	7.35±2.29
$\mathbf{A_6}$	43.9±3.6	6.57±4.73	7.90±2.41	1.31±1.83
$\mathbf{A_7}$	29.9±1.2	21.4±1.7	9.52±2.16	10.6±3.5
BT	38.4±3.1	/	/	/
TC	30.2±1.5	/	61.2±2.6	36.4±2.3

718 **Table 2.** Antimicrobial assays of title molecules **B_1–B_5** toward pathogens *Xoo* and

719 *Xac in vitro*.

Compounds	*Xoo*				*Xac*			
	Inhibition rate (100%)		Regression equation	EC_{50} (μg/mL)	Inhibition rate (100%)		Regression equation	EC_{50} (μg/mL)
	50 μg/mL	25 μg/mL			100 μg/mL	50 μg/mL		
A_1	100	100	y=5.74x−0.69	9.77±0.18	43.8±3.0	25.7±2.1	/	/
B_1	100	84.6±1.2	y=6.48x−2.46	14.1±0.26	100	70.7±8.6	y=2.20x+2.13	19.9±0.3
B_2	100	100	y=3.52x+2.01	7.03±0.23	88.8±0.3	57.3±0.6	y=4.77x−2.73	41.7±0.8
B_3	90.1±1.0	72.7±1.3	y=3.40x+0.45	21.7±0.9	76.1±4.1	58.9±1.9	y=2.38x+0.96	49.7±0.3
B_4	73.4±3.3	42.1±2.4	y=1.64x+2.56	31.0±2.7	73.0±2.3	57.4±1.3	y=1.52x+2.60	37.8±0.3
B_5	11.8±2.1	7.41±1.71	/	/	11.6±1.1	0	/	/
BT	38.4±3.1	/	y=1.50x-2.05	92.6±2.1	/	/	/	/
TC	30.2±1.5	/	y=1.54x+1.79	121.8±3.6	61.2±2.6	36.4±2.3	y=2.15x+0.94	77.0±2.0

720

721 **Table 3.** Antimicrobial assays of title molecules **C_1–C_7**, **D_1–D_7**, and **E_1–E_7** toward

722 pathogens *Xoo* and *Xac in vitro*.

Compds	*Xoo*				*Xac*			
	Inhibition rate (100%)		Regression equation	EC_{50} (μg/mL)	Inhibition rate (100%)		Regression equation	EC_{50} (μg/mL)
	50 μg/mL	25 μg/mL			100 μg/mL	50 μg/mL		
C_1	100	100	y=5.68x+0.15	7.13±0.16	88.2±0.5	74.8±1.9	y=2.64x+1.63	18.6±0.4
D_1	100	92.6±1.4	y=4.25x+0.30	12.7±0.1	100	71.4±1.7	y=2.64+1.69	17.9±0.2
E_1	100	89.1±0.7	y=5.79x–1.29	12.1±0.1	100	91.8±1.5	y=2.99x+1.43	15.6±0.2
C_2	100	96.2±0.3	y=4.86x–0.12	11.2±0.4	97.4±1.9	87.5±1.2	y=2.64x+1.80	16.2±0.1
D_2	98.3±0.9	47.7±1.0	y=7.30x–5.45	26.9±0.3	100	65.5±1.9	y=6.05x−4.44	36.3±0.3
E_2	100	94.0±2.4	y=6.71x–2.50	13.0±0.3	100	91.4±4.1	y=2.32x+2.38	13.5±0.3
C_3	6.36±2.38	2.19±2.07	/	/	13.6±1.2	8.00±4.81	/	/
D_3	99.4±0.2	79.9±2.6	y=4.02x+0.51	13.1±0.2	94.5±1.4	63.8±0.8	y=2.48x+1.54	24.8±1.9
E_3	95.2±2.0	55.7±2.2	y=8.91x–6.96	21.9±0.2	49.6±1.8	42.7±0.4	/	/
C_4	99.1±0.2	80.2±0.3	y=2.50x+2.39	11.1±0.5	37.6±2.2	22.4±1.6	/	/
D_4	25.3±3.7	0	/	/	48.9±3.7	33.0±2.9	/	/
E_4	98.5±0.4	72.7±0.5	y=8.33x−4.59	14.1±0.8	99.3±0.7	93.0±1.4	y=2.42x+2.55	10.3±0.3
C_5	97.2±0.2	54.1±5.7	y=7.81x−5.81	24.1±1.1	98.6±0.1	83.3±1.8	y=6.30x-5.03	39.0±0.9
D_5	100	100	y=4.60x+0.37	10.1±0.3	100	100	y=2.99x+1.34	16.7±1.2
E_5	100	100	y=5.69x−0.40	8.89±0.25	100	69.1±2.2	y=3.51x+0.18	23.6±1.9
C_6	100	100	y=2.88x+2.52	7.24±0.17	91.5±0.3	88.6±1.2	y=2.24x+2.39	14.6±0.5
D_6	96.1±0.3	86.5±0.8	y=2.15x+2.98	8.75±0.36	97.7±0.3	70.5±1.6	y=4.14x−1.36	34.2±1.2
E_6	97.2±0.4	96.1±0.2	y=3.01x+2.37	7.44±0.17	98.1±0.3	74.0±3.7	y=2.30x+1.76	26.7±1.1
C_7	20.6±2.9	16.6±1.2	/	/	48.6±2.7	24.6±0.9	/	/
D_7	36.3±2.5	25.4±1.3	/	/	12.2±1.0	8.63±1.44	/	/
E_7	76.6±1.1	38.6±3.2	y=3.35x−0.05	32.0±1.6	79.3±2.0	62.4±0.8	y=2.79x+0.32	47.6±1.3
BT	38.4±3.1	/	y=1.50x−2.05	92.6±2.1	/	/	/	/
TC	30.2±1.5	/	y=1.54x+1.79	121.8±3.6	61.2±2.6	36.4±2.3	y=2.15x+0.94	77.0±2.0

723

724 **Table 4.** *In vivo* control efficacy of **B_2** and **C_1** (drug dosage: 200 μg/mL, 14 days after

725 spraying) against rice bacterial blight.

Treatment	Curative effect			Protective effect		
	Morbidity (%)	Disease index (%)	Control efficiency (%)[b]	Morbidity (%)	Disease index (%)	Control efficiency (%)[b]
B_2	100	37.93	51.55	100	39.26	49.84
C_1	100	39.91	49.02	100	37.44	52.17
BT	100	47.02	39.94	100	46.79	40.23
TC	100	45.69	41.63	100	47.53	39.29
CK[a]	100	78.31	/	100	78.31	/

726 [a]Negative control. [b]Statistical analysis was conducted using ANOVA under equal variances assumed ($P > 0.05$) and equal

727 variances not assumed ($P < 0.05$).

728

729 **Figures**

730 **Figure 1**

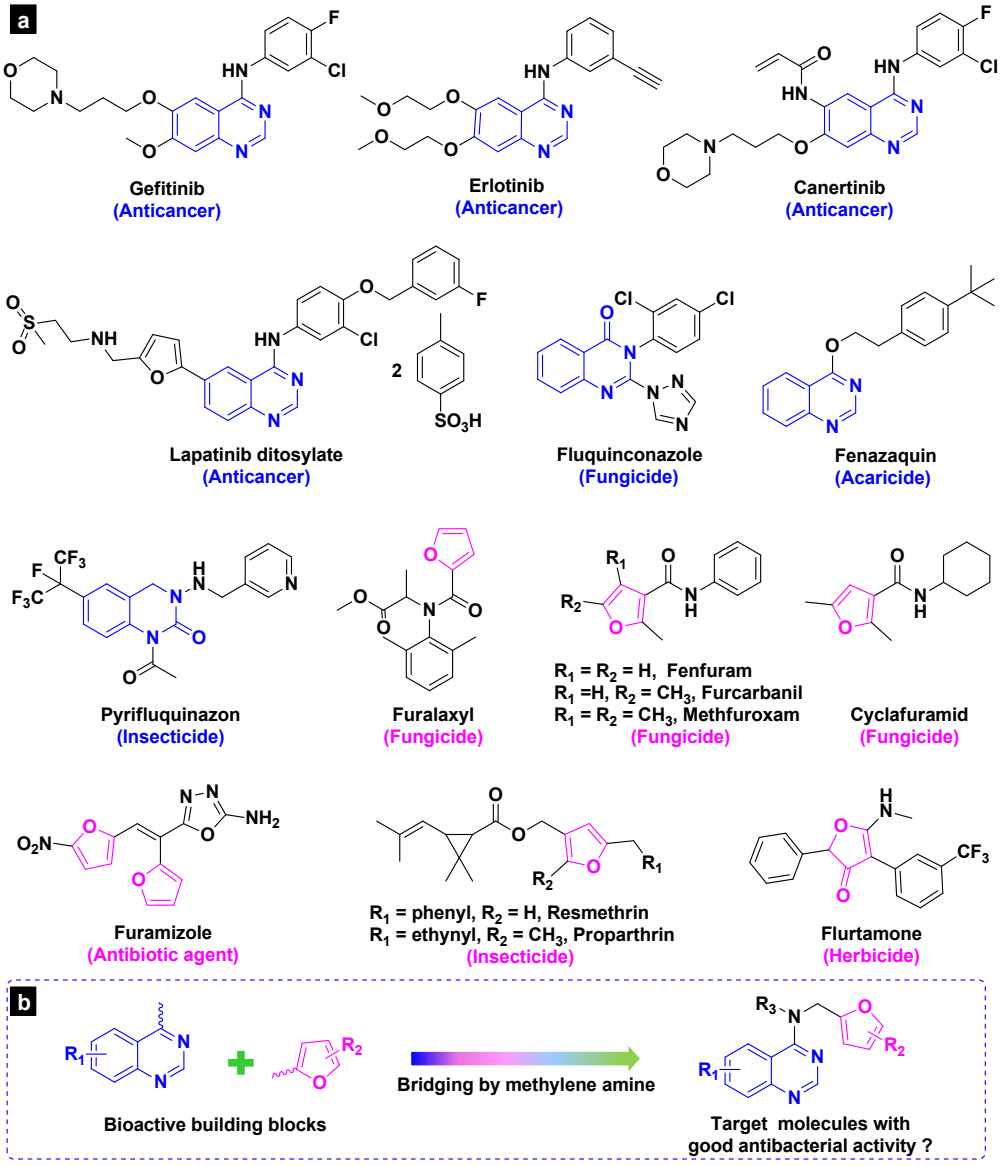

731

732

733 **Figure 2**

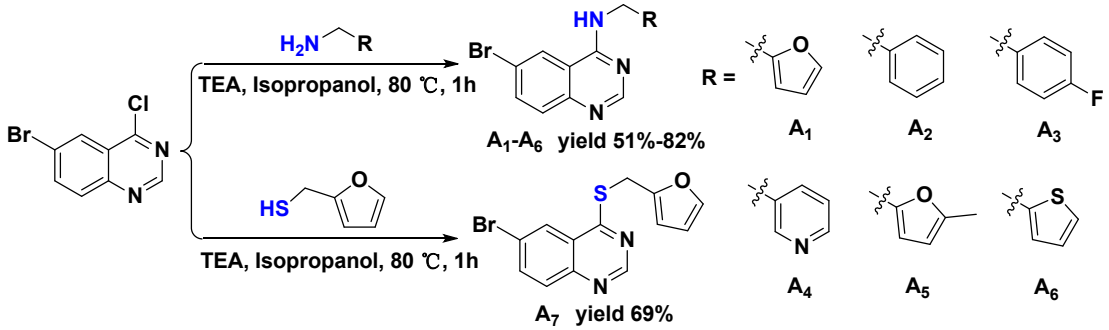

734

735

736 **Figure 3**

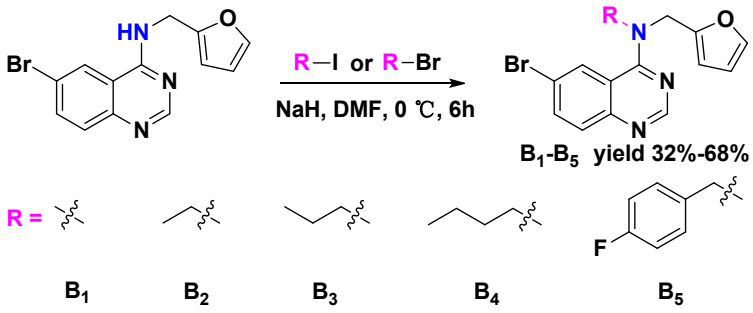

737

738

739 **Figure 4**

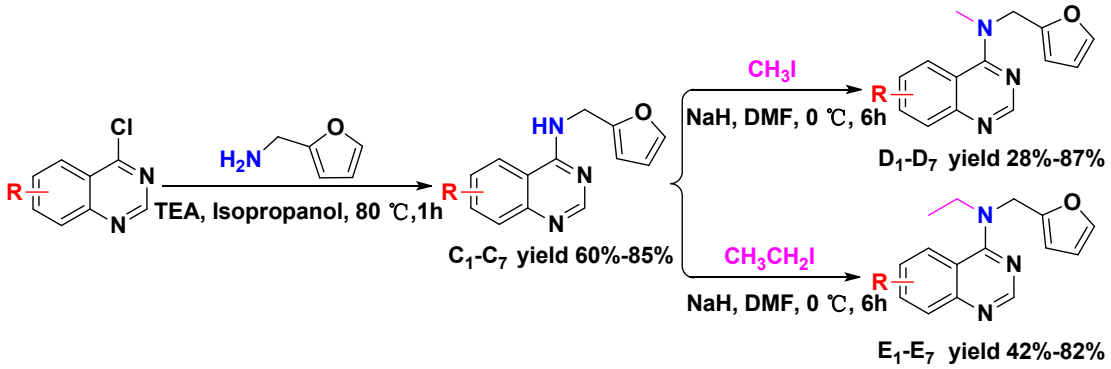

R = 6-Cl: C_1, D_1, E_1 R = 5-Cl: C_2, D_2, E_2 R = 7-Cl: C_3, D_3, E_3 R = 8-Cl: C_4, D_4, E_4

740 R = H: C_5, D_5, E_5 R = 6-CH_3: C_6, D_6, E_6 R = 6,7-diOCH_3: C_7, D_7, E_7

741

742 **Figure 5**

743

744

745 **Figure 6**

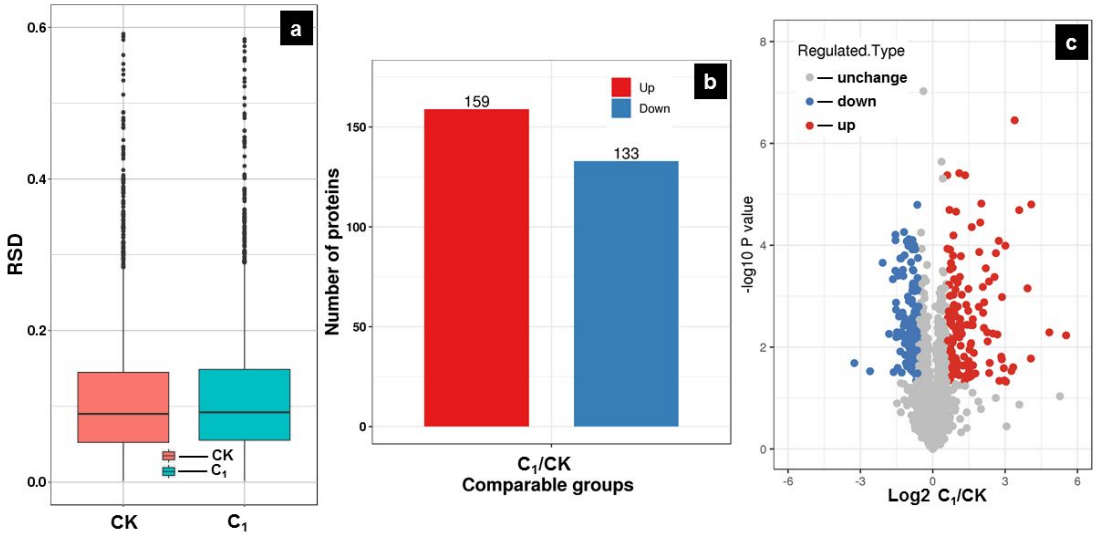

746

747

748 **Figure 7**

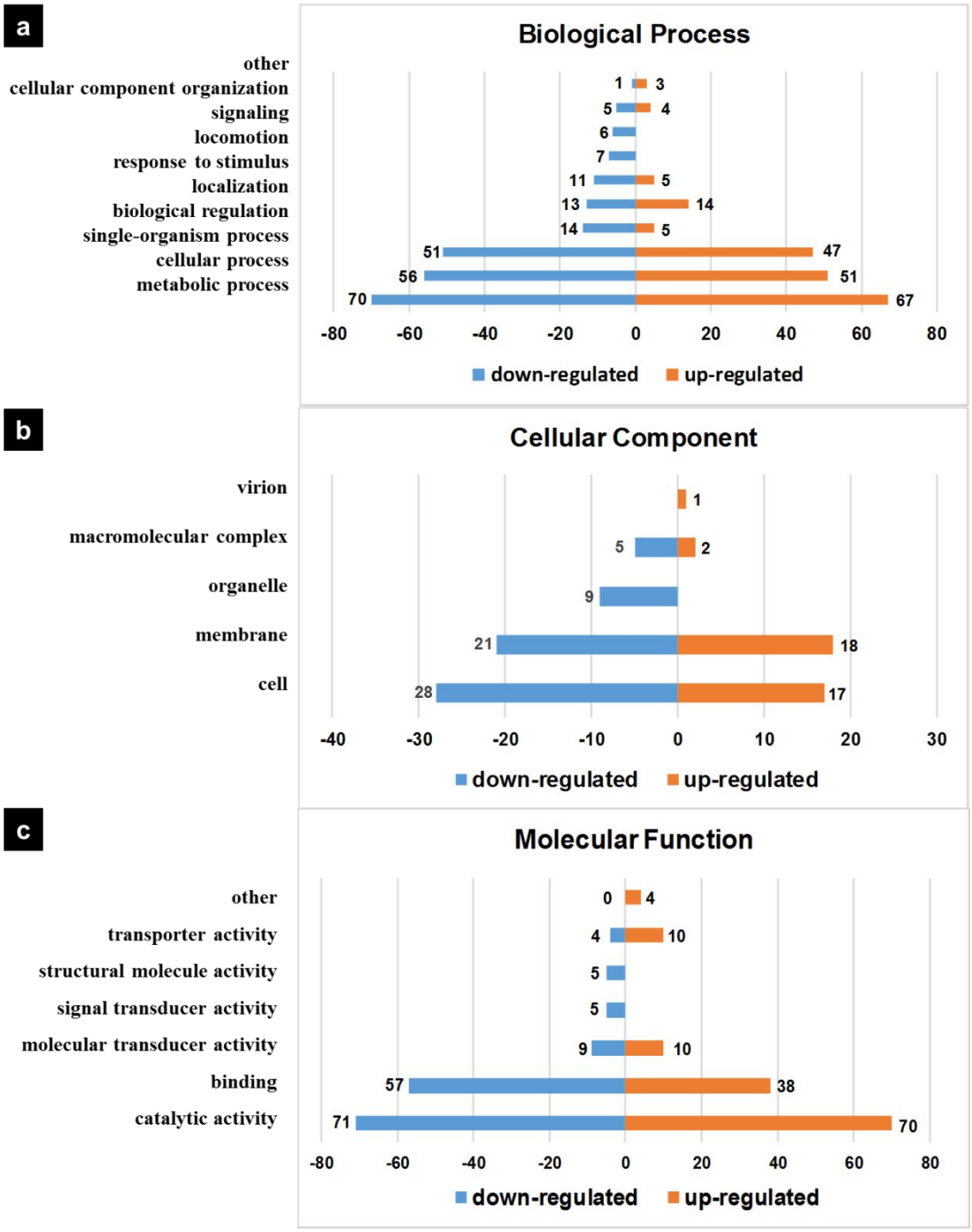

749

750

751 **Figure 8**

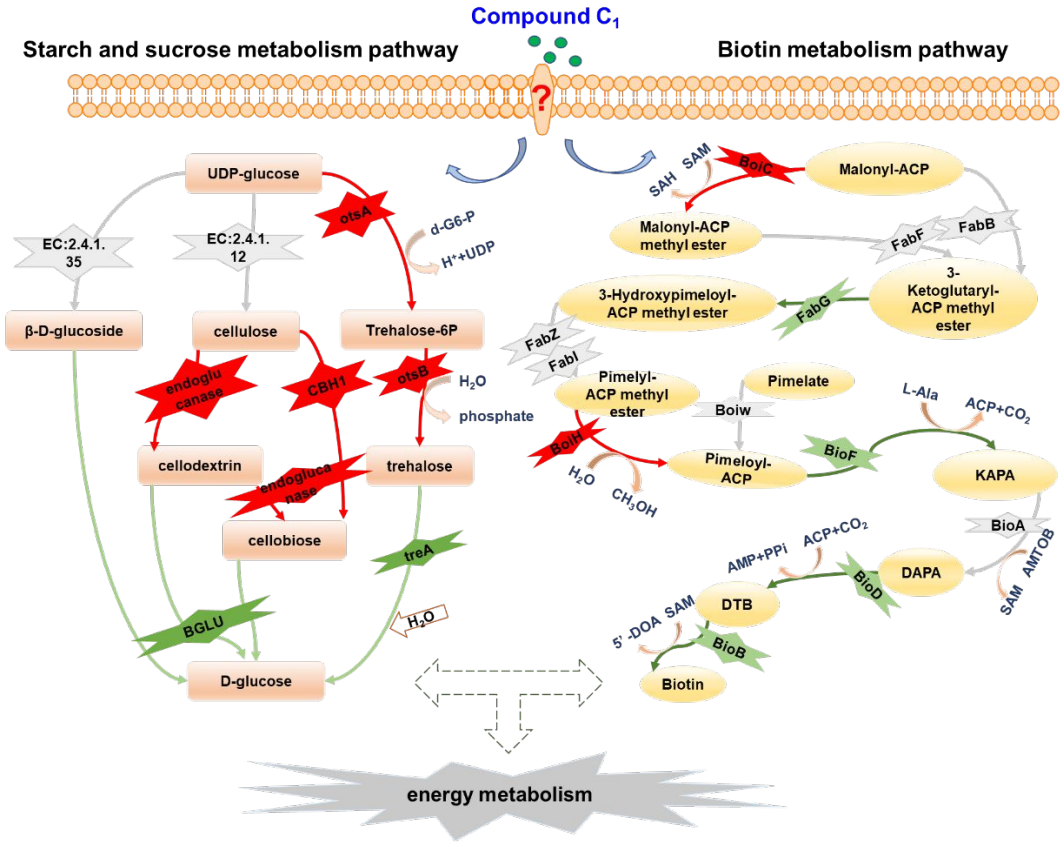

752

753

754 **Figure 9**

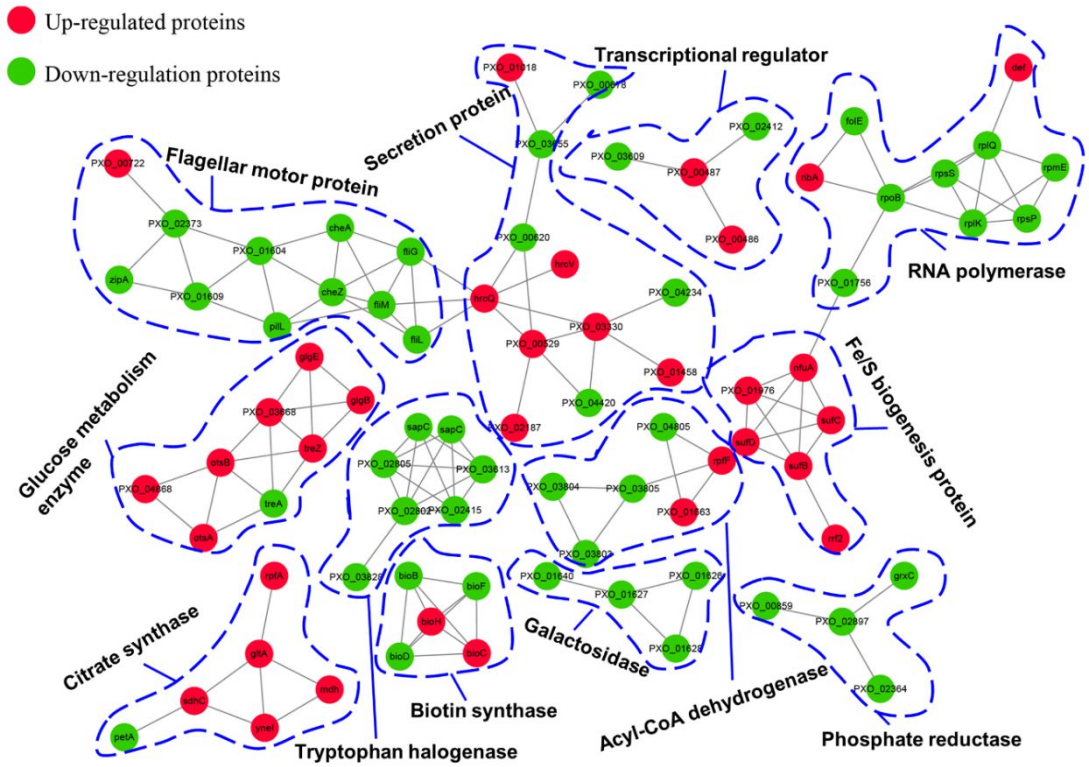

755

756

757 **Figure 10**

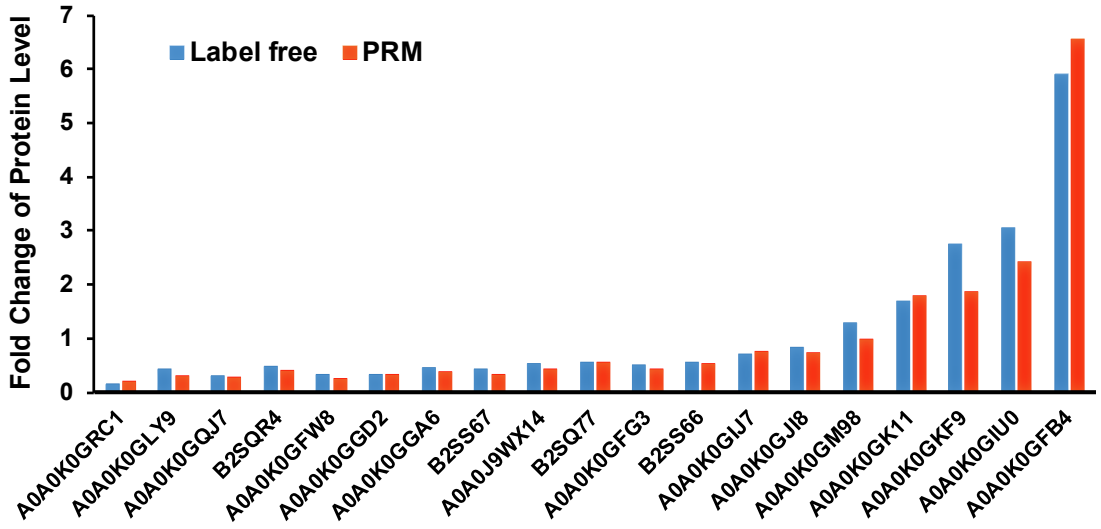

758

759

760 **Figure 11**

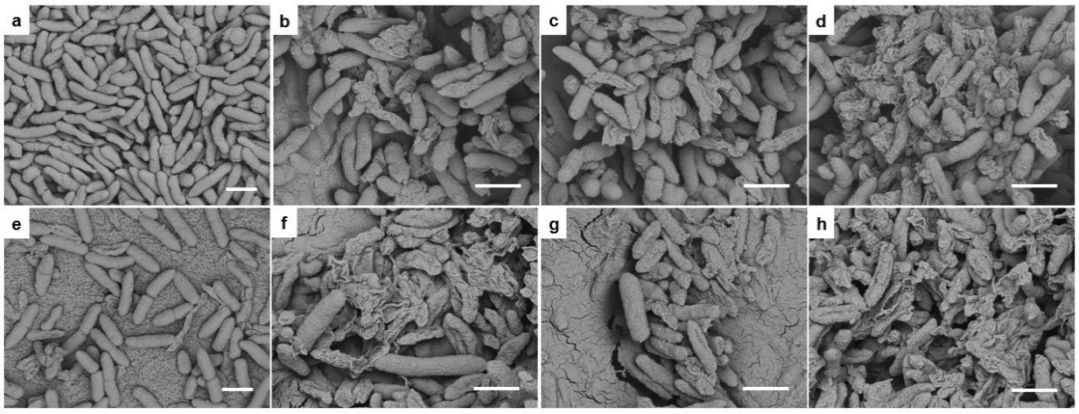

761

762

763 **Figure 12**

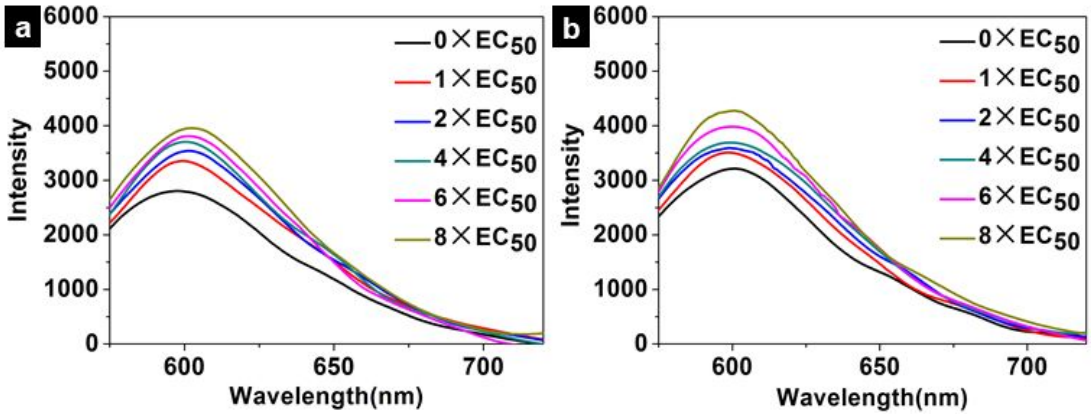

764

765

766 **Graphic for Table of Contents**

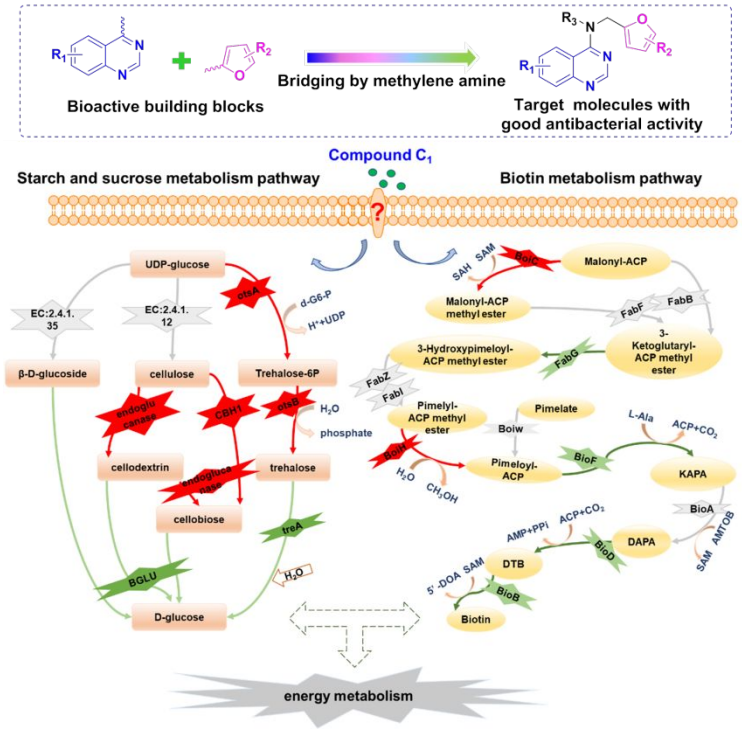

767

768